Spin States

International Edition: DOI: 10.1002/anie.201810161
German Edition: DOI: 10.1002/ange.201810161

High-Pressure Synthesis of $A_2NiO_2Ag_2Se_2$ (A = Sr, Ba) with a High-Spin Ni^{2+} in Square-Planar Coordination

*Yuki Matsumoto, Takafumi Yamamoto, Kousuke Nakano, Hiroshi Takatsu, Taito Murakami, Kenta Hongo, Ryo Maezono, Hiraku Ogino, Dongjoon Song, Craig M. Brown, Cédric Tassel, and Hiroshi Kageyama**

Abstract: *Square-planar coordinate Ni^{2+} ions in oxides are exclusively limited to a low-spin state ($S=0$) owing to extensive crystal field splitting. Layered oxychalcogenides $A_2Ni^{II}O_2Ag_2Se_2$ (A = Sr, Ba) with the $S=1$ NiO_2 square lattice are now reported. The structural analysis revealed that the Ni^{2+} ion is under-bonded by a significant tensile strain from neighboring Ag_2Se_2 layers, leading to the reduction in crystal field splitting. $Ba_2NiO_2Ag_2Se_2$ exhibits a G-type spin order at 130 K, indicating fairly strong in-plane interactions. The high-pressure synthesis employed here possibly assists the expansion of NiO_2 square lattice by taking the advantage of the difference in compressibility in oxide and selenide layers.*

Layered oxychalcogenides and oxypnictides comprising of alternate stacking of oxide layers and chalcogenide/pnictide layers have shown interesting properties.[1] For example, the FeAs layer in LaOFeAs is responsible for high-T_c superconductivity, where the charge reservoir LaO layer controls the doping levels by aliovalent substitution.[2] Excellent thermoelectric properties in BiOCuSe are achieved by combining a high electronic conductivity in the CuSe layer with a low thermal conductivity in the BiO layer.[3,4]

A layered compound $A_2MO_2M'_2X_2$ (A = Ba, Sr, Ca; M, M′ = transition metal; X = chalcogen, pnictogen) has MO_2 square-lattice sheets, sandwiched by M'_2X_2 layers.[1] Although superconductivity has not been reported, the absence of apical ligands in the MO_2 layer, which is crucial to optimize T_c values for cuprates,[5,6] offers an ideal platform to study physical properties intrinsic to the square lattice. So far, MO_2 layers with $S=5/2$, and $S=3/2$ have been realized, respectively, by $M=Mn^{II}$ (for example, $Sr_2MnO_2Zn_2As_2$),[7,8] Co^{II} (for example, $SrCoO_2Cu_2S_2$).[9] Of particular importance is the $S=1$ square lattice for which strong quantum fluctuations are expected. Unfortunately, the Ni^{II} ions in this family (for example, $Sr_2NiO_2Cu_2S_2$)[10] and other square-planar coordinate oxides such as $LaNiO_{2.5}$[11] and $BaNiO_2$[12] exclusively adopt a low-spin state ($S=0$) owing to extensive crystal field splitting. Herein, we show that $A_2NiO_2Ag_2Se_2$ (A = Sr, Ba), prepared under high pressure (along with $Ba_2CuO_2Ag_2Se_2$ and $Ba_2MnO_2Ag_2Te_2$), afford a high-spin state and thus the $S=1$ square lattice (Figure 1). The origin of the high-spin state is discussed in terms of a tensile strain from Ag_2Se_2 layers, which could be greatly enhanced by high-pressure synthesis.

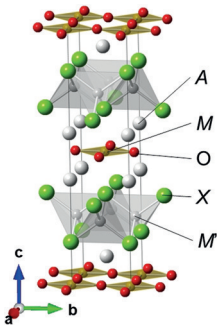

Figure 1. Structure of $A_2MO_2M'_2X_2$ (A = Ba, Sr, Ca; M, M′ = transition metal; X = chalcogen, pnictogen).

Powder samples of $Ba_2MO_2Ag_2Se_2$ (M = Ni, Cu) were prepared under 7 GPa at 850 °C using a stoichiometric mixture of BaO, Ni, Cu, Ag and Se. The XRD patterns (Figure 2) were readily indexed using a body-centered tetragonal (bct) cell with $a=4.21554(7)$ Å and $c=20.1965(6)$ Å for M = Ni and $a=4.2248(1)$ Å and $c=20.135(1)$ Å for M = Cu. These patterns resemble with that of $Ba_2CoO_2Ag_2Se_2$[13] with the $I4/mmm$ space group (Figure 2, bottom). No impurity was seen for M = Cu, while tiny unknown peaks were detected for M = Ni. No peaks associated with superstructures as observed in $Ba_2ZnO_2Ag_2Se_2$[14] were found. Likewise, the XRD pattern of $Sr_2NiO_2Ag_2Se_2$, synthesized at 5 GPa and 850 °C, was mainly indexed by the bct cell ($a=4.09460(8)$ Å, $c=19.2733(8)$ Å), with additional reflections from SrSe and unknown impurities (Supporting Information, Figure S1). All synthetic attempts under ambi-

[*] Y. Matsumoto, Dr. T. Yamamoto, Dr. H. Takatsu, T. Murakami, Dr. C. Tassel, Prof. H. Kageyama
Graduate School of Engineering, Kyoto University
Kyoto 615-8510 (Japan)
E-mail: kage@scl.kyoto-u.ac.jp
Dr. K. Nakano, Prof. K. Hongo, Prof. R. Maezono
School of Information Science, JAIST
Asahidai 1-1, Nomi, Ishikawa 923-1292 (Japan)
Prof. K. Hongo
Research Center for Advanced Computing Infrastructure, JAIST
Asahidai 1-1, Nomi, Ishikawa 923-1292 (Japan)
and
National Institute for Materials Science
Tsukuba 305-0047 (Japan)
and
PRESTO (Japan)
Prof. K. Hongo, Prof. R. Maezono
Computational Engineering Applications Unit. RIKEN
2-1 Hirosawa, Wako. Saitama 351-0198 (Japan)
Dr. H. Ogino, Dr. D. Song
Electronics and Photonics Research Institute, AIST
Ibaraki 305-8568 (Japan)
Dr. C. M. Brown
Center for Neutron Research, NIST
Gaithersburg, MD 20899-6102 (USA)
Supporting information and the ORCID identification number(s) for the author(s) of this article can be found under: https://doi.org/10.1002/anie.201810161.

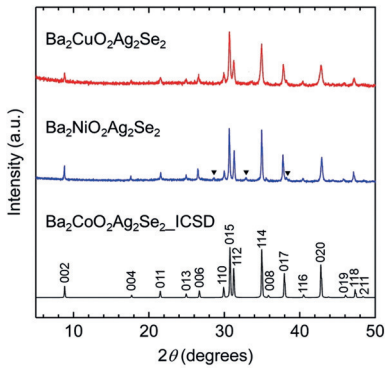

Figure 2. Powder XRD patterns of $Ba_2MO_2Ag_2Se_2$ (M = Ni, Cu). A simulated pattern of $Ba_2CoO_2Ag_2Se_2$[13] is shown for comparison. Triangles denote unknown impurity peaks.

ent pressure failed (Supporting Information, Figure S2), suggesting a metastable nature of these phases. All compounds are semiconducting.

We carried out Rietveld analysis on the synchrotron XRD data for the Ag-based systems (Figure 3) assuming the $Sr_2Mn_3Sb_2O_2$ structure (*I*4/*mmm*). The unknown peaks for $Sr_2NiO_2Ag_2Se_2$ were excluded from analysis (Supporting Information, Figure S3). No appreciable Ag deficiency was recognized within the accuracy of refinements, though M′-site deficiency (ca. 25%) is sometimes found, such as in $Sr_2MnO_2Ag_{1.5}Se_2$.[15] For $Ba_2CuO_2Ag_2Se_2$, a large atomic displacement parameter U_{iso} of 0.02 Å^2 was obtained for Cu at the 2*a* site, which led us to locate at the 8*i* site. This yielded an acceptable value of about 0.4 Å^2. Such displacement was not seen for M = Ni. The final results are shown in Figure 3 and the Supporting Information, Figure S4 and Table S1.

The Ag–Se bonds in the Ag_2Se_2 slabs of $Ba_2NiO_2Ag_2Se_2$, $Sr_2NiO_2Ag_2Se_2$ and $Ba_2CuO_2Ag_2Se_2$ are 2.76 Å, 2.75 Å and 2.71 Å, being similar to those in $Sr_2CoO_2Ag_2Se_2$,[15] $Ba_2CoO_2Ag_2Se_2$,[13] and LaOAgSe[16] (2.74–2.76 Å). By contrast, the M–O bonds in the MO_2 square lattice (that is, *a*/2) are significantly elongated: the Ni–O bonds of 2.13 Å for Ba and 2.05 Å for Sr are much longer than any compounds with Ni^{II} in square-planar coordination, for example $Sr_2Ni^{II}O_2Cl_2$ (2.02 Å),[17] $Sr_2Ni^{II}O_2Cu_2S_2$ (1.96 Å),[1,10] and $LaNi^{II}O_{2.5}$ (1.89 Å).[11] Even a monovalent nickel in $LaNi^{I}O_2$ has a shorter Ni–O bond of 1.98 Å.[18] The mean Cu–O distance of 2.11 Å in $Ba_2CuO_2Ag_2Se_2$ is also noteworthy since so far the longest distance among oxides with CuO_4 square-planar coordination was 2.09 Å in $InBa_2CuO_{4.5\pm\delta}$.[19] This elongation causes displacement of the Cu atom toward one oxygen atom, making Cu three-coordinate (d_{Cu-O} = 1.87 Å × 1, 2.12 Å × 2, 2.35 Å × 1). While the bond valence sum (BVS) values of Ag and Ba/Sr well agree with their formal valences (Supporting Information, Table S2),[20] those for Cu and Ni are found extremely low: 1.19, 1.25, and 1.31 for $Ba_2NiO_2Ag_2Se_2$, $Sr_2NiO_2Ag_2Se_2$ and $Ba_2CuO_2Ag_2Se_2$, showing the underbonded nature of Ni–O/Cu–O.

A telluride counterpart has not been reported. Figure S5 (Supporting Information) shows a successful formation of $Ba_2MnO_2Ag_2Te_2$ (prepared at 2 GPa and 850 °C) with *a* = 4.39060(4) Å and *c* = 20.6918(2) Å (Supporting Information, Table S1). The Mn–O distance of 2.20 Å is even longer than 2.13 Å for $Ba_2MnO_2Ag_2Se_2$ with the longest Mn–O bond.[13]

In square-planar coordinate nickel oxides,[10–12] the Ni^{II} ion is subject to intense crystal field, making it exclusively a low spin (*S* = 0) state, as shown in Figure 4a. However, once Ni–O bonds are elongated, the anti-bonding $d_{x^2-y^2}$ level will be stabilized, which may eventually lead to a high-spin state (Figure 4b). In fact, the magnetic susceptibility of $Ba_2NiO_2Ag_2Se_2$ (Figure 5a) clearly demonstrates that this

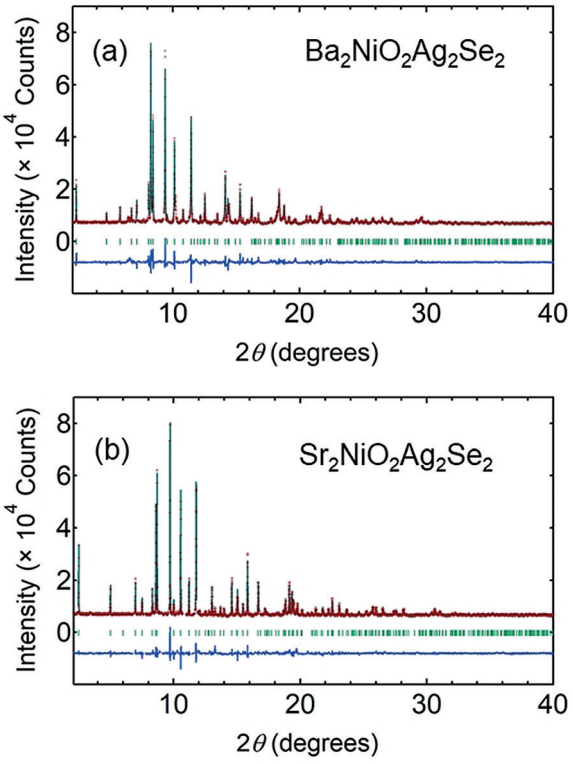

Figure 3. Observed and calculated synchrotron XRD (λ = 0.42073(1) Å) patterns for a) $Ba_2NiO_2Ag_2Se_2$ and b) $Sr_2NiO_2Ag_2Se_2$ at room temperature. Red crosses: observed, green lines: calculated, and blue lines: difference intensities; green ticks are the peak positions.

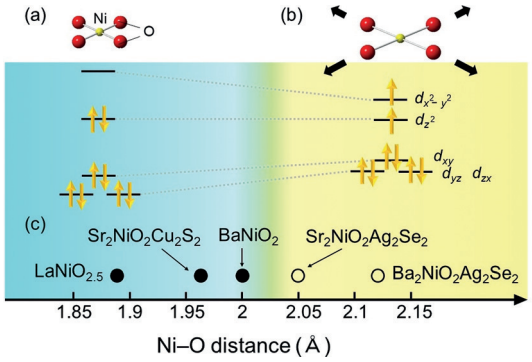

Figure 4. Crystal-field splitting and electronic configurations of Ni 3d orbitals in square-planar coordination for a) low spin (*S* = 0) and b) high spin (*S* = 1) states. c) Correlation between Ni–O distance and spin state. Solid and open circles, respectively, represent *S* = 0[1,11,12] and *S* = 1 (this study). Note that according to BVS, the ideal Ni^{II}–O/Cu^{II}–O distances for square planar coordination are 1.91/1.935 Å.[22]

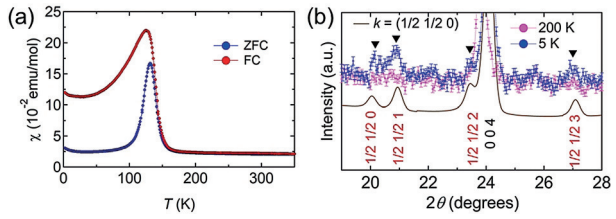

Figure 5. a) Magnetic susceptibility and b) PND for $Ba_2NiO_2Ag_2Se_2$ at 200 K and 5 K. The solid line is a simulated pattern with the G-type spin structure.

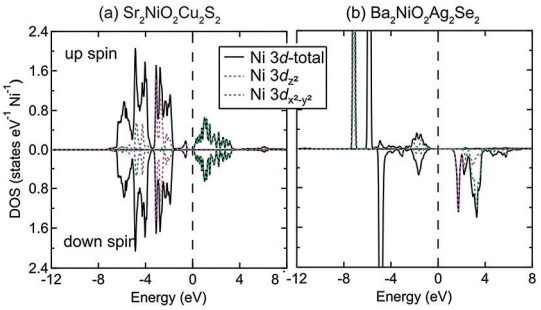

Figure 6. Partial DOSs of Ni $3d_{total}$, d_{z^2}, and $d_{x^2-y^2}$ for a) $Sr_2NiO_2Cu_2S_2$ and b) $Ba_2NiO_2Ag_2Se_2$ (see the Supporting Information, Figures S13 and S14 for details).

nickelate is magnetic; a steep increase below about 150 K followed by a maximum at around 130 K implies magnetic order to a canted antiferromagnetic state (see details in the Supporting Information). Powder neutron diffraction (PND) pattern at 5 K (Figure 5b) exhibits magnetic reflections assigned with a propagation vector of (1/2, 1/2, 0). Because of limited intensities and resolution, we simulated a magnetic pattern, where Ni moments were assumed to align perpendicular to [001] as expected from magnetic HOMO–LUMO interactions (Supporting Information, Figure S8),[21] and obtained a reasonable agreement for $S=1$ (Figure 5b; Supporting Information, Figure S9). The occurrence of G-type spin order at 130 K, despite the long interlayer distance (ca. 10 Å), indicates strong in-plane antiferromagnetic interactions.

The magnetic ground state of $Sr_2NiO_2Ag_2Se_2$ is also evident; the Curie–Weiss fitting above 150 K gave an effective magnetic moment of $P_{eff}=2.97\ \mu_B$ (thus consistent with $S=1$), along with a Weiss temperature of −158 K (Supporting Information, Figure S7). A complex χ–T curve below 40 K implies a certain magnetic transition, but the absence of magnetic reflections at 6 K (Supporting Information, Figure S12) indicates a spin-glass state, as found in $Sr_2CoO_2M'_2Se_2$ (M′ = Cu, Ag)[15] and $A_2MnO_2Zn_2As_2$.[22] The difference in the ground state between $Ba_2NiO_2Ag_2Se_2$ and $Sr_2NiO_2Ag_2Se_2$ may be ascribed to that in the interlayer interactions.

Figure 4c suggests that a spin crossover from a low-spin to high-spin state occurs at a critical Ni–O distance between 2.00 Å and 2.05 Å. A high spin state is reported in $Sr_2NiO_2Cl_2$ with $d_{Ni\text{-}O}=2.02$ Å,[17] but the apical chlorine ligands have a substantial contribution to the BVS (0.30) and hence to crystal field splitting (CFS). In contrast, the BVS for Se (×2) in $A_2NiO_2Ag_2Se_2$ is less than 0.05. Since Se is in general a weaker ligand field than O,[23,24] and the Ni–Se distance of 3.3 Å is much longer than typical cases (ca. 2.6 Å), the contribution of Se to CFS would be much smaller. Note that it is not straightforward to extract the effect of splitting from calculation (see details in the Supporting Information).

DFT calculations provided a further justification of high spin state for $Ba_2NiO_2Ag_2Se_2$. Figure 6 shows partial DOSs from $Sr_2NiO_2Cu_2S_2$ for $S=0$ and $Ba_2NiO_2Ag_2Se_2$ for $S=1$, as a starting model. The calculations for $Sr_2NiO_2Cu_2S_2$ (Figure 6a) gave $d_{Ni-O}=1.95$ Å and a non-magnetic state with empty $3d_{x^2-y^2}$ orbital and the band gap (BG) of 0.2 eV. In $Ba_2NiO_2Ag_2Se_2$, this model yielded $d_{Ni-O}=2.10$ Å and the magnetic (G-type) ground state with BG = 0.8 eV, where d_{z^2}/$d_{x^2-y^2}$ orbitals of only the up-spin channel are occupied (Figure 6b). On the contrary, models with a high/low spin state for $Sr_2NiO_2Cu_2S_2$/$Ba_2NiO_2Ag_2Se_2$ resulted in metallic states, both of which contradict with experimental observations. Given the bottom of the conduction band in $Ba_2NiO_2Ag_2Se_2$ consisting mainly of Ni 3d orbital (Supporting Information, Figure S13), electron doping to the NiO_2 layer by chemical substitution is of interest by analogy with cupric superconductors.

Clearly, the expanded MO_2 square lattice in the four compounds is enabled by a large tensile strain from the neighboring Ag_2Se_2 or Ag_2Te_2 layers, with an additional contribution from A cations. Then, a natural question that arises is what makes the present phases accessible by high pressure synthesis. Possibly, the high pressure is advantageous for stabilizing a compound with a MO_2 square-planar slab due to facile contraction perpendicular to the plane, as shown in $SrFeO_2$[25] and Sr_2MO_4 (M = Cu, Pd).[26] Another possibility, which seems more relevant, is that under the synthetic condition (that is, high pressure) the size mismatch between Ag_2Se_2 and MO_2 layers could be in an acceptable range, owing to a large difference in compressibility of the two layers. Conversely, the mismatch would be too large to form these compounds under ambient condition. To support this, chalcogenide (S^{2-}, Se^{2-}, Te^{2-}) anions are approximately twice compressible than an oxide anion (O^{2-}), as seen in rock-salt SrX (X = O, S, Se, Te): bulk modulus of SrSe is 45 GPa while that of SrO is 91 GPa.[27] Once these compounds are formed under high pressure and high temperature, upon pressure release (after quenching temperature), the Ag_2Se_2 layer expands significantly, providing a large tensile strain to the MO_2 sheet. Thus, the use of high pressure could be a useful strategy to tune the bond length of MO_2 lattice more extensively than otherwise possible.

Acknowledgements

This work was supported by KAKENHI (JP16H06438-40, JP16K21724, JP16H02267) and CREST (JPMJCR1421), JSPS Core-to-Core Program (A). Synchrotron and neutron experiments were performed at SPring-8 (2016A1050, 2016A1043) and NIST.

Conflict of interest

The authors declare no conflict of interest.

Keywords: high-pressure synthesis · oxychalcogenide · spin states · square lattice · strain

How to cite: *Angew. Chem. Int. Ed.* **2019**, *58*, 756 – 759
Angew. Chem. **2019**, *131*, 766 – 769

[1] a) S. J. Clarke, P. Adamson, S. J. C. Herkelrath, O. J. Rutt, D. R. Parker, M. J. Pitcher, C. F. Smura, *Inorg. Chem.* **2008**, *47*, 8473 – 8486; b) H. Kageyama, K. Hayashi, K. Maeda, J. P. Attfield, Z. Hiroi, J. M. Rondinelli, K. R. Poeppelmeier, *Nat. Commun.* **2018**, *9*, 772.
[2] Y. Kamihara, T. Watanabe, M. Hirano, H. Hosono, *J. Am. Chem. Soc.* **2008**, *130*, 3296 – 3297.
[3] L.-D. Zhao, J. He, D. Berardan, Y. Lin, J.-F. Li, C.-W. Nan, N. Dragoe, *Energy Environ. Sci.* **2014**, *7*, 2900 – 2924.
[4] S. K. Saha, *Phys. Rev. B* **2015**, *92*, 041202(R).
[5] H. Kotegawa, Y. Tokunaga, K. Ishida, G.-q. Zheng, Y. Kitaoka, H. Kito, A. Iyo, K. Tokiwa, T. Watanabe, H. Ihara, *Phys. Rev. B* **2001**, *64*, 64515.
[6] H. Mukuda, Y. Yamaguchi, S. Shimizu, Y. Kitaoka, P. Shirage, A. Iyo, *J. Phys. Soc. Jpn.* **2008**, *77*, 124706.
[7] R. Nath, V. O. Garlea, A. I. Goldman, D. C. Johnston, *Phys. Rev. B* **2010**, *81*, 224513.
[8] S. L. Brock, S. M. Kauzlarich, *J. Alloys Compd.* **1996**, *241*, 82 – 88.
[9] C. F. Smura, D. R. Parker, M. Zbiri, M. R. Johnson, Z. A. Gál, S. J. Clarke, *J. Am. Chem. Soc.* **2011**, *133*, 2691 – 2705.
[10] K. Otzschi, H. Ogino, J. Shimoyama, K. Kishio, *J. Low Temp. Phys.* **1999**, *117*, 729 – 733.
[11] M. T. F. J. A. Alonso, M. J. Martínez-Lope, J. L. García-Muñoz, *J. Phys. Condens. Matter* **1997**, *9*, 6417 – 6426.
[12] M. Matsuda, K. Katsumata, A. Zheludev, S. M. Shapiro, G. Shirane, *J. Phys. Chem. Solids* **1999**, *60*, 1121 – 1123.
[13] T. Zhou, Y. Wang, S. Jin, D. Li, X. Lai, T. Ying, H. Zhang, S. Shen, W. Wang, X. Chen, *Inorg. Chem.* **2014**, *53*, 4154 – 4160.
[14] S. J. C. Herkelrath, I. Saratovsky, J. Hadermann, S. J. Clarke, *J. Am. Chem. Soc.* **2008**, *130*, 14426 – 14427.
[15] S. Jin, X. Chen, J. Guo, M. Lei, J. Lin, J. Xi, W. Wang, W. Wang, *Inorg. Chem.* **2012**, *51*, 10185 – 10192.
[16] D. O. Charkin, A. V. Urmanov, S. M. Kazakov, *J. Alloys Compd.* **2012**, *516*, 134 – 138.
[17] Y. Tsujimoto, C. I. Sathish, Y. Matsushita, K. Yamaura, T. Uchikoshi, *Chem. Commun.* **2014**, *50*, 5915 – 5918.
[18] M. A. Hayward, M. A. Green, M. J. Rosseinsky, J. Sloan, *J. Am. Chem. Soc.* **1999**, *121*, 8843 – 8854.
[19] T. Shimada, S. Kambe, S. Ohshima, N. Ohnishi, K. Hiraga, *Phys. C* **1997**, *287*, 935 – 936.
[20] N. E. Brese, M. O'Keeffe, *Acta Crystallogr. Sect. B* **1991**, *47*, 192 – 197.
[21] M. H. Whangbo, E. E. Gordon, H. Xiang, H. J. Koo, C. Lee, *Acc. Chem. Res.* **2015**, *48*, 3080 – 3087.
[22] T. C. Ozawa, S. M. Kauzlarich, *Chem. Mater.* **2001**, *13*, 973 – 980.
[23] S. E. Livingstone, *Q. Rev. Chem. Soc.* **1965**, *19*, 386 – 425.
[24] J. M. Zadrozny, J. Telser, J. R. Long, *Polyhedron* **2013**, *64*, 209 – 217.
[25] T. Kawakami, Y. Tsujimoto, H. Kageyama, X. Q. Chen, C. L. Fu, C. Tassel, A. Kitada, S. Suto, K. Hirama, Y. Sekiya, Y. Makino, T. Okada, T. Yagi, N. Hayashi, K. Yoshimura, S. Nasu, R. Podloucky, M. Takano, *Nat. Chem.* **2009**, *1*, 371 – 376.
[26] T. Yamamoto, Z. Li, C. Tassel, N. Hayashi, M. Takano, M. Isobe, Y. Ueda, K. Ohoyama, K. Yoshimura, Y. Kobayashi, H. Kageyama, *Inorg. Chem.* **2011**, *50*, 11787 – 11794.
[27] H. Luo, R. G. Greene, A. L. Ruoff, *Phys. Rev. B* **1994**, *49*, 341 – 343.

Manuscript received: September 4, 2018
Revised manuscript received: October 22, 2018
Accepted manuscript online: November 15, 2018
Version of record online: December 17, 2018

